ACS APPLIED MATERIALS & INTERFACES

Research Article

www.acsami.org

Hydrothermal Synthesis of Boron and Nitrogen Codoped Hollow Graphene Microspheres with Enhanced Electrocatalytic Activity for Oxygen Reduction Reaction

Zhongqing Jiang,[†] Xinsheng Zhao,[‡] Xiaoning Tian,[†] Lijuan Luo,[†] Jianghua Fang,[†] Haoqi Gao,[†] and Zhong-Jie Jiang*[,§]

[†]Department of Chemical Engineering, Ningbo University of Technology, Ningbo 315016, China

[‡]School of Physics and Electronic Engineering, Jiangsu Normal University, Xuzhou 221116, China

[§]New Energy Research Institute, College of Environment and Energy, South China University of Technology, Guangzhou 510006, China

S Supporting Information

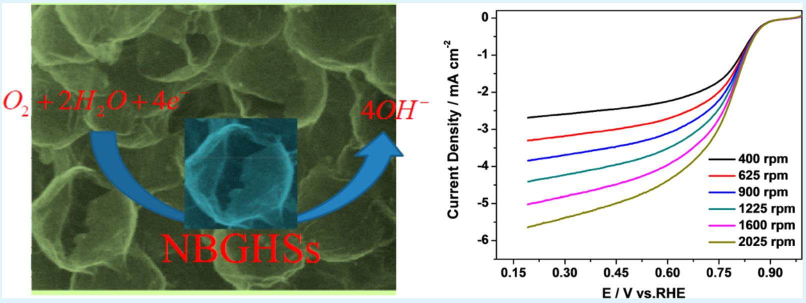

ABSTRACT: Boron and nitrogen codoped hollow graphene microspheres (NBGHSs), synthesized from a simple template sacrificing method, have been employed as an electrocatalyst for the oxygen reduction reaction (ORR). Because of their specific hollow structure that consists of boron and nitrogen codoped graphene, the NBGHSs can exhibit even high electrocatalytic activity toward ORR than the commercial JM Pt/C 40 wt %. This, along with their higher stability, makes the NBGHSs particularly attractive as the electrocatalyst for the ORR with great potential to replace the commonly used noble-metal-based catalysts.

KEYWORDS: *hydrothermal synthesis, boron and nitrogen codoping, hollow graphene microspheres, template sacrificing, oxygen reduction reaction*

INTRODUCTION

The development of cathodic electrocatalysts that could promote oxygen reduction reaction (ORR) has received a great deal of attention in the recent years due to their potentials to improve the performance of fuel cells and metal−air batteries.[1−4] The traditional fuel cells and metal−air batteries use noble-metal-based nanoparticles, such as Pt and its alloys, as the catalysts for the ORR.[5−7] Although the noble-metal-based nanoparticles have long been considered as the most active electrocatalysts for the ORR, their intrinsic limitations, such as high cost, susceptibility to the crossover of fuel molecules and CO poisoning, scarcity in nature, etc., have greatly hindered their widespread uses in the fuel cell and metal−air battery technologies.[8−11] Recent efforts have therefore been devoted to the development of nonprecious metal or metal-free catalysts to circumvent the problems associated with noble-metal-based materials.[2,12−18]

Among various electrocatalysts reported to date, nitrogen doped carbon has in particular received significant attention due to its competitive ORR electrocatalytic activity.[19−23] The experimental observations and quantum mechanics calculations have attributed the high electrocatalytic activity of nitrogen doped carbon to the electron accepting ability of the nitrogen atoms, which created a net negative charge on the adjacent carbon atoms, facilitating the adsorption of oxygen and attraction of electrons from the anode for the reduction of oxygen.[24−26] Recent work has also addressed the use of boron doped carbon as the electrocatalyst for the ORR.[27−29] The larger difference between the electronegativity of oxygen and boron atoms makes the adsorption of oxygen on boron dopants much easier.[27−29] The electrochemical results showed that boron doped carbon could exhibit greatly enhanced catalytic activity toward ORR.[27,30] Compared to the singly doped counterparts, carbon materials codoped with two or more heteroatoms are receiving growing attention.[19,28,31−35] One can expect that the codoped materials could not only possess the

Received: June 23, 2015
Accepted: August 17, 2015
Published: August 17, 2015

DOI: 10.1021/acsami.5b05585

properties of their singly doped counterparts but also produce novel and unique properties that originate from collective interactions between dopants. Studies have demonstrated that codoped carbon materials could exhibit significantly improved electrocatalytic activities, with respect to their singly doped counterparts, due to a synergetic effect arising from the codoping.[19,28,36−38]

Besides electrocatalytic activities, fuel cells and metal−air batteries also require use of electrically conductive cathodic ORR catalysts with high specific surface areas to achieve high electrochemical performance.[4,14,39,40] This has led to investigation of heteroatom doped graphene as the electrocatalysts for the ORR due to its superior electric conductivity.[13,28,34] However, heteroatom doped graphene may not meet the requirement of high specific surface area, because the high aspect ratio of its graphitic structure makes heteroatom doped graphene readily aligned in a layered architecture with a low specific surface area due to strong van der Waals and $\pi-\pi$ interactions between the graphitic planes.[13,41] Methods used to improve the specific surface area of heteroatom doped graphene include fabrication of them into a three-dimensonal porous structure.[14,19,34,42] In such a three-demensonal porous structure, doping makes heteroatom doped graphene electrocatalytically active for the ORR, whereas its graphitic structure makes it highly conductive for electron conduction. This, along with the high specific surface area that makes it more accessible to the ORR, leads to the three-demensonal porous heteroatom doped graphene materials with significantly higher electrochemical performance for the ORR, as indeed demonstrated in some recently published work.[41−44]

Compared with conventional porous graphene materials, graphene hollow spheres might be of particular interest due to their high surface-to-volume ratio, superior electrical conductivity, low density, as well as excellent mass transport features.[16,45] In this sense, the fabrication of heteroatom codoped graphene hollow spheres might be a promising way to produce ORR catalysts with high electrochemical performance. To demonstrate this, we reported here on the synthesis of nitrogen and boron codoped graphene hollow microspheres (NBGHSs) using a template sacrificing method, which were then used as the electrocatalyst for the ORR. The results showed that these NBGHSs were highly active for the ORR. Their high electrochemical performance could be attributed to the N, B codoped graphitic structure and the specific microspherical hollow morphology, which make them more active for oxygen adsorption and reduction and promote more surface area accessible to the ORR, respectively.

■ EXPERIMENTAL SECTION

Synthesis of Porous SiO_2 Spheres. The porous SiO_2 spheres used as the sacrificing templates for the synthesis of the NBGHSs were fabricated using a procedure reported previously.[46] Typically, 13.2 g of aqueous ammonia (32 wt %, 0.25 mol) and 60.0 g of absolute ethanol (EtOH, 1.3 mol) were first added to 50 g of deionized water containing 2.5 g of *n*-hexadecyltrimethylammonium bromide ($C_{16}TMABr$, 0.007 mol). The obtained mixture was then stirred for 15 min, followed by addition of 4.7 g of TEOS, which resulted in a gel with the molar ratio of TEOS:$C_{16}TMABr:NH_3H_2O$:EtOH = 1:0.3:11:144:58. The reaction lasted for 2 h. The thus-formed white precipitate was filtered and washed with 100 mL of deionized water and 100 mL of methanol. After drying overnight at 363 K, the solid product was heated to 823 K in air and kept at that temperature for 5 h.

Scanning electron microscopy (SEM) showed that the obtained porous SiO_2 spheres were mostly spherically shaped with an average size of ∼500 nm.

Fabrication of Amino-Modified SiO_2 Nanoparticles. ∼1 g of SiO_2 particles obtained above was dispersed into dry toluene (300 mL) under ultrasonication to form a suspension. 3-Aminopropyltrimethoxysilane (3 mL) was then added. The obtained solution was heated at a temperature of 65 °C for 12 h, which led to the formation of amino-modified SiO_2 nanoparticles (NH_2-SiO_2) after washing and drying under vacuum. The NH_2-SiO_2 particles were redispersed in water by ultrasonication for uses.

Fabrication of the NBGHSs. For the fabrication of the NBGHSs@NH_2-SiO_2 composites with a core/shell structure, 0.3 g of NH_2-SiO_2 was first dispersed in 30.0 mL of distilled water. The pH value of the solution was then adjusted to 2.5 by adding 1.0 M HCl solution. To this solution was added 20 mL of 2.0 mg mL^{-1} negatively charged GO suspension (GO was prepared from the natural graphite flakes using a modified Hummers method as described elsewhere[47,48]). The obtained mixture was stirred at room temperature for 24 h, which led to the wrapping of GO onto NH_2-SiO_2 through an electrostatic interaction. After that, 18 mmol ammonia boron trifluoride (NH_3BF_3) was added into the above GO wrapped NH_2-SiO_2 solution, and the mixture was stirred again at room temperature. The resulting stable suspension, sealed in a Telfon-lined autoclave, was hydrothermally treated at 180 °C for 12 h. Finally, the as-prepared sample was freeze-dried overnight, followed by vacuum drying at 60 °C for several hours.

To obtain the NBGHSs, the NBGHSs@NH_2-SiO_2 spheres synthesized above were then calcined in Ar atmosphere at 420 °C for 2 h and subsequently calcined in Ar atmosphere at 800 °C for 30 min to improve the conductivity. The obtained product was cooled to room temperature and doubly washed with a 10 wt % aqueous HF solution to remove the silica template. The final product was washed thoroughly with an acetone−water mixture and then with deionized water until the conductivity of the filtrate reached to 10 μS.

The GHSs were prepared using the same synthetic procedure for the synthesis of the NBGHSs without using dopants. The same synthetic procedure was also used for the synthesis of the NGHSs and the BGHSs with addition of appropriate dopants as needed. For example, the syntheses of the NGHSs and BGHSs, urea and boric acid (H_3BO_3) were employed, respectively.

Characterization. An environmental scanning electron microscope (Model Quanta 650 FEG) at an operation voltage of 20.0 kV was employed to measure the morphology of the obtained samples. TEM measurements were conducted on a JEM-2100F high-resolution transmission electron microscope with an accelerating voltage of 200 kV. The chemical composition of the samples was determined by X-ray photoelectron spectroscopy (XPS) on a VG ESCALAB 250 spectrometer (Thermo Electron, U.K.), using an Al Kα X-ray source (1486 eV). XRD was performed on a Scintag XDS 2000 X-ray powder diffractometer with monochromatized CuKa radiation (λ = 1.5418 Å); the data were collected between scattering angles (2θ) of 10 and 80 °C. Raman spectra were collected with a Renishaw inVita Raman spectrometer with an excitation wavelength of 514.5 nm (2.41 eV) from an argon ion laser. The laser power on the sample was kept below 1 mW to avoid possible laser-induced heating and the exposure time was ∼5 s. A laser beam size of ∼1 μm with a 100× objective lens was used. The specific surface areas of the samples were analyzed by a surface area analyzer (NOVA 2000, Quantachrome) using physical adsorption/desorption of N_2 at the liquid-N_2 temperature. Specific surface area was calculated according to the Brunauer−Emmett−Teller (BET) method.

Electrochemical Measurement. Cyclic voltammetry was performed using a computer-controlled potentiostat (CHI 760C, CH Instrument, USA) with a typical three-electrode cell, in which a saturated calomel electrode (SCE), a platinum wire, and a glassy carbon electrode/rotating disk electrode (RDE) loaded with various catalysts were employed as the reference electrode, the counter-electrode, and the working electrode, respectively. All the experiments were carried out in 0.1 M KOH at room temperature (25 °C). For the preparation of the working electrode, 5.0 mg of as-synthesized catalyst was mixed with 50 μL of Nafion solution (5.0% Nafion in ethanol), 450 μL of DI water, and 500 μL of isopropyl alcohol. The mixture was sonicated and 5.0 μL of suspension was applied onto an electrode (5 mm diameter) and then fully dried. For a comparison, the commercially available Johnson Matthey (JM) Pt/C 40 wt % (Johnson Matthey Corp., Pt loading: 40 wt % Pt on the carbon) electrode was also prepared. The Pt/C suspension was prepared by dispersing 10 mg of the Pt/C powder in 2 mL of ethanol in the presence of 50 μL of isopropyl alcohol solution with 5 wt % Nafion. The addition of a small amount of Nafion could effectively improve the dispersion of the Pt/C catalyst suspension and prevent its droping from the electrode during the electrochemical measurements. For the RDE measurements, catalyst inks were prepared by the same method as CV's. 5 μL of ink (containing 25 μg catalyst) was loaded on a glassy carbon rotating disk electrode of 5 mm in diameter (Pine Instruments) giving a loading of 0.13 mg/cm^2. The working electrode was scanned cathodically at a rate of 5 mV s^{-1} with varying rotating speeds from 400 to 2025 rpm. Koutecky−Levich plots were analyzed at various electrode potentials. The slopes of their best linear fit lines were used to calculate the number of electrons transferred on the basis of the Koutecky−Levich equation. The scan rate was 5 mV s^{-1} for both cyclic voltammetry and rotating disk electrode measurements. The geometrical surface area of the glassy carbon electrode (19.6 mm^2) was used to calculate the current density. The potentials reported in this work were referenced to the reversible hydrogen electrode (RHE) through RHE calibration.[8,49] In 0.1 M KOH, E (RHE) = E (SCE) + 0.992 V, as demonstrated by the calibration curve given in the Supporting Information (as shown in Figure S1).

RESULTS AND DISCUSSION

Figure 1a shows a typical SEM image of the NBGHSs fabricated based on a procedure involving the synthesis of the amine functionalized SiO$_2$ particles (NH$_2$−SiO$_2$), the adsorption of the negatively charge GO onto the surface of the positively charge NH$_2$−SiO$_2$, the doping of the NH$_2$−SiO$_2$ supported GO with N and B using the hydrothermal method in the presence of NH$_3$BF$_3$, and the subsequent removal of NH$_2$−SiO$_2$ through the HF etching. Complying with the template of the NH$_2$−SiO$_2$ particles used for their fabrication, most of the NBGHSs remain a spherical shape with an average diameter of ~500 nm (as shown in Figure 1a). This indicates that the removal of the SiO$_2$ template would not change the microspherical shape of the NBGHSs. Their hollow structure could be identified by some collapsed NBGHSs as marked by the red boxes in Figure 1a. The hollow structure of the NBGHSs could also be demonstrated by their TEM image shown in Figure 1b, where the NBGHSs appear as translucent pancakes with opaque peripheries, similar to the TEM images of the hollow particles reported previously.[50−53] The presence of collapsed particles in the TEM of the NBGHSs suggests the fragmentation of some NBGHSs, indicating the highly pliable nature of the graphitic structure may not well support the specific hollow morphology of some NBGHSs, which could be destroyed by the ultrasonication and mechanical stirring during the washing and sample preparation for TEM imaging. This could further be demonstrated by the presence of some distorted NBGHSs in their SEM and TEM images given in Figure 1a,b.

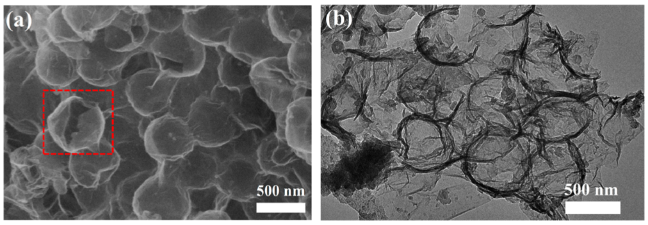

Figure 1. (a) SEM and (b) TEM images of the NBGHSs.

The XPS survey spectrum in Figure 2a shows the presence of C, N, B, and O atoms in the NBGHSs. This is different from the XPS spectrum of the GHSs (synthesized from the same synthetic procedure for the fabrication of the NBGHSs without using the dopants), where only C and O atoms are detected. The spectra deconvolution in Figure 2b shows that the asymmetric N 1s peak could be fitted into five peaks at binding energy of 397.5, 398.3, 400.0, 401.1, and 403.4 eV, corresponding to the B−N, pyridinic N, pyrrolic N, graphitic N, and oxidized N, respectively.[30,37,54−56] This is similar to the deconvoluted spectrum of B 1s shown in Figure 2c, where six peaks corresponding to B$_4$C (187.9 eV), B-doped carbon (188.8 eV), B−C (sp^2) (189.6 eV), C−BN/C−BO (190.6 eV), C−BNO (191.4 eV), and C−BO$_2$ (192.5 eV) could be clearly identified.[29,30,55,57] These results are in good agreement with the XPS spectra of the conventional N and B codoped graphene (NBG) reported previously,[37,55] suggesting that N and B have been doped into the NBGHSs during the hydrothermal process and subsequent calcination reaction. This can further be supported by the C 1s spectrum of the NBGHSs shown in Figure 2d, where distinguishable peaks attributable to the chemical environments of carbon atoms bonded to carbon, nitrogen, and boron in graphene can be clearly observed.[30,55,57,58] The appearance of N and B components at the different oxidation states could be attributed to the complexity of the pyrolytic reactions between the different oxygenous groups of GO (such as carboxyl, hydroxyl, and epoxy oxygen groups) and NH$_3$BF$_3$ during the hydrothermal process, which facilitates the incorporation of N and B into the graphitic structure of GO at the different oxidation states. The dominance of the graphitic carbon, as demonstrated by the deconvoluted C 1s spectrum in Figure 2d, indicates that the hydrothermal reaction product of the NBGHSs remains a graphitic structure. This is in good agreement with their Raman spectrum shown in Figure 3a, where two prominent peaks corresponding to the D band (arising from the disordered sp^2 hybridized carbon) and G band (associated with the tangential stretching mode of highly ordered pyrolytic graphite) could be clearly identified. The relatively higher I_D/I_G ratio (1.35) of the NBGHSs compared to that of the GHSs (I_D/I_G = 1.05) could be attributed to the codoping of N and B, both of which could increase disorder of the graphitic structure of the NBGHSs, as demonstrated by the previously published work[28,29,38] and the higher I_D/I_G ratios of the NGHSs (I_D/I_G = 1.14) and the BGHSs (I_D/I_G = 1.29) shown in Figure 3a (the synthesis of the NGHSs and BGHSs were performed through the same synthetic procedure for the fabrication of the NBGHSs using urea and boric acid (H$_3$BO$_3$) as the dopant, respectively). Worthnoting is that the NBGHSs and the BGHSs contain higher contents of oxygen atoms in comparison to the GHSs and the NGHSs, as demonstrated by the XPS survey spectra shown in Figure 2a and the elemental analyses presented in Table S1. These excess oxygen could be attributed to the adsorbed molecular oxygen on the surface of the NBGHSs, indicating that the introduction of B would increase the adsorption of the NBGHSs to oxygen, due to the increased polarization and electron deficiency of the graphitic structure induced by the B-doping. The high adsorption of the NBGHSs to oxygen could be a fascinating feature for their potential uses

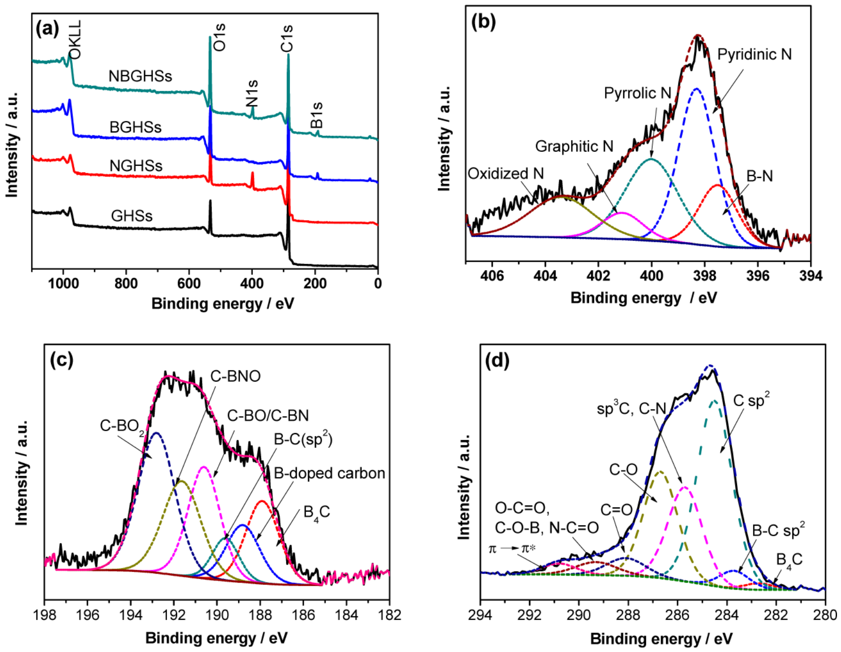

Figure 2. (a) XPS spectra of the GHSs, the BGHSs, the NGHSs, and the NBGHSs. Deconvoluted (b) N 1s, (c) B 1s, and (d) C 1s spectra of the NBGHSs.

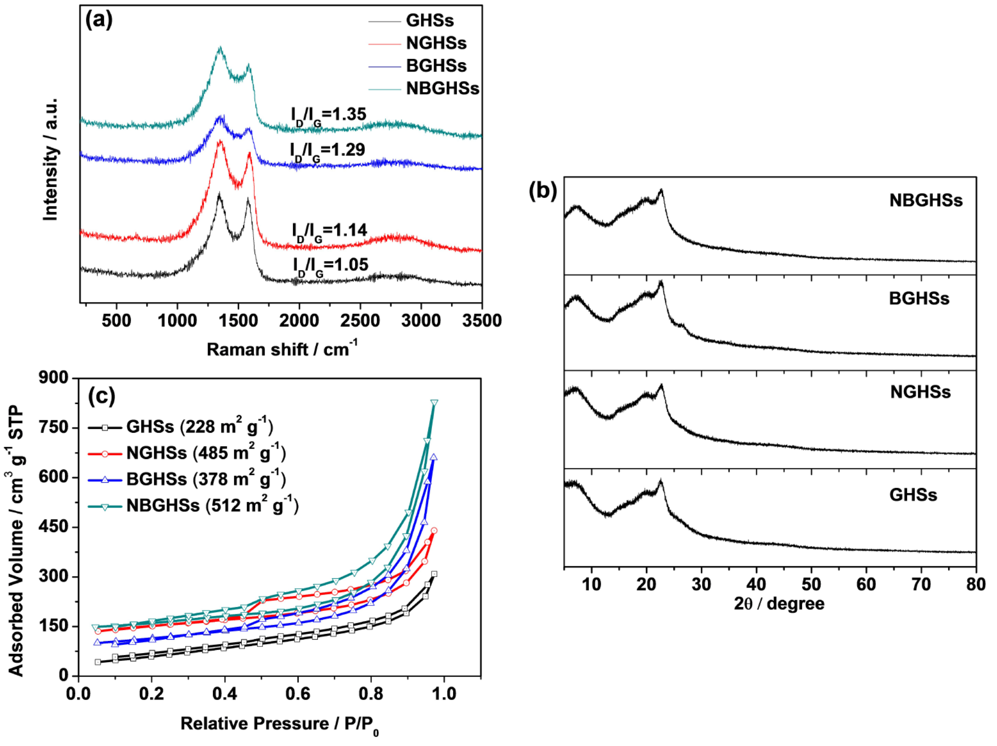

Figure 3. (a) Raman spectra of the GHSs, the BGHSs, the NGHSs, and the NBGHSs. Their corresponding ratios of I_D/I_G are given in the figure. (b) XRD patterns of the GHSs, the BGHSs, the NGHSs, and the NBGHSs. (c) N_2 adsorption−desorption isotherms of the GHSs, the BGHSs, the NGHSs, and the NBGHSs. The specific surface areas of the samples are given in the figure, which were calculated using the Brunauer−Emmett−Teller (BET) method with the adsorption data at the relative pressure (P/P_0) range of 0.05−0.30.

as the electrocatalysts for ORR, because the adsorption of oxygen to the electrocatalyst surface has been identified as an important step in the ORR.

The XRD pattern of the NBGHSs exhibits a peak at 2θ = 22.6°, which could be assigned to the (001) reflection of the graphitic structure of the NBGHSs. The broad peak and the high baseline in the small 2θ angle observed in Figure 3b may suggest that the graphitic structure in the wall of the NBGHSs is not well aligned. This is consistent with the SEM and TEM images in Figure 1, where the distortion and fragmentation of some NBGHSs have been observed. The similarity of the XRD pattern of the NBGHSs with those of the GHSs, the NGHSs and the BGHSs indicates that they possess the same structure, which could also be demonstrated by the TEM and SEM

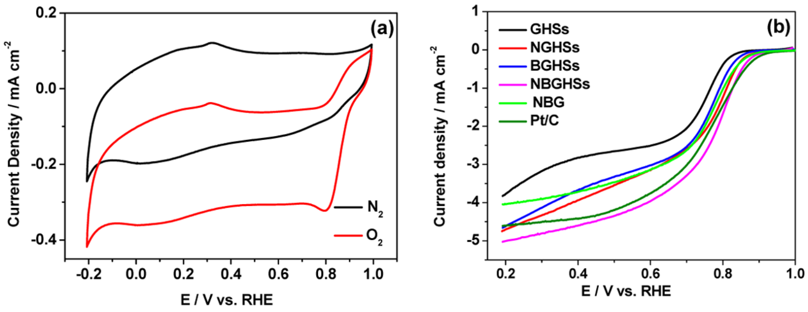

Figure 4. (a) CV curves of the NBGHSs in 0.1 M KOH solution saturated with N_2 or O_2 at a scan rate of 5 mV s^{-1}. (b) LSVs for the ORR on the GHSs, the NGHSs, the BGHSs, the NBG, Pt/C, and the NBGHSs in an O_2-saturated 0.1 M KOH solution at a scan rate of 5 mV s^{-1}.

images of the GHSs, the NGHSs, the BGHSs, and the NBGHSs shown in Figure 1 and S2, respectively. This is because that all of them were synthesized from the same synthetic procedure with only using different dopants or without using dopants.

The N_2 adsorption−desorption isotherms of the NBGHSs are given in Figure 3c, where a type IV adsorption−desorption behavior can be identified. The uptake of N_2 at relatively higher pressure ($P/P_0 > 0.9$) in the N_2 adsorption−desorption isotherm suggests the existence of macropores, which is in good agreement with their microspherical hollow morphology. The specific surface area of the NBGHSs calculated using the multipoint Brunauer−Emmett−Teller (BET) method is 512 m^2 g^{-1}, which is larger than those of a number of graphene-based materials reported to date.[59,60] This indicates the fabrication of the graphene-based materials into the microspherical shape could increase their specific surface area due to the reduction of the layer-by-layered alignment of the graphitic planes. Although the N_2 adsorption−desorption isotherms of the GHSs, the NGHSs, and the BGHSs exhibits similar adsorption−desorption profiles to those of the NBGHSs, their specific surface areas are much lower (as indicated in Figure 3c), suggesting that the doping of both N and B could greatly increase the specific surface area of the NBGHSs. This is consistent with the fact that the doping of N and B into the NBGHSs produces more edge atoms, which increase their specific surface area because the lateral sides of the edge atoms could also contribute to the N_2 adsorption.[61]

The reactivity of the NBGHSs toward oxygen reduction was first evaluated by cyclic voltammetry (CV) in 0.1 M KOH solution saturated with N_2 or O_2. Figure 4a shows that the CV curve of the NBGHSs in the N_2 saturated solution exhibits featureless voltammetric currents within the potential ranging from −0.2 to +1.0 V. This is different from the CV curve of the NBGHSs in the O_2 saturated solution where a distinct cathodic peak centered at 0.80 V can be observed, which clearly demonstrates the electrocatalytic activity of the NBGHSs toward ORR. Although the GHSs, the NGHSs, the BGHSs, and the NBG are also electrochemically active for the ORR, their activities are much lower than that of the NBGHSs, as demonstrated by their CVs in Figure 4a and Figure S3 in the Supporting Information. The linear sweep voltamograms (LSVs) in Figure 4b, measured by the rotating disk electrode, show that the NBGHSs exhibit even higher limiting current density and more positive half-wave potential ($E_{1/2}$, i.e., the potential at which the current is half of the limiting current) for the ORR than the JM Pt/C 40 wt % (a commercialized electrocatalyst for ORR with higher activity), although the onset potentials of the ORR for the both catalysts appear at the relatively same position. This indicates that the NBGHSs could be used as a highly active electrocatalyst for the ORR with great potential to replace the conventional noble-metal-based catalysts. The XPS spectrum shown in Figure 2a indicates the presence of only C, B, N, and O in the NBGHSs with no other elements detected, which clearly rules out the possibility that the high electrocatalytic activity of the NBGHSs originates from the impurities, which might be formed from the chemicals used for the synthesis of the NBGHSs. This is well consistent with the experimental procedure in which the products produced in each step for the synthesis of the NBGHSs were well washed.

To understand well the origin of the higher electrocatalytic activity of the NBGHSs, the electrocatalytic behaviors of the GHSs, the NGHSs, the BGHSs and the conventional N, B codoped graphene (NBG) (the NBG was synthesized using a procedure reported previously[55]) toward ORR are also investigated. Figure 4b shows that the GHSs exhibit low electrochemical performance for the ORR, as demonstrated by their relatively low limiting current density and less positive onset and half-wave potentials. The higher limiting current densities and more positive onset and half-wave potentials for the ORR observed in the LSVs of the NGHSs and the BGHSs, in comparison to those in the LSV of the GHSs, suggest that the doping of the GHSs with N and B could both increase the electrocatalytic activity of the GHSs toward ORR. This result indicates that the higher electrocatalytic activity of the NBGHSs is the combining result of the N and B doping, which could further be demonstrated by the observation that the NBGHSs exhibit higher electrocatalytic activity than both of the NGHSs and the BGHSs. In addition, the results in Figure 4b also show that the electrocatalytic activity of the NBGHSs is much higher than that of the conventional NBG, although both of them are doped with the comparable N and B. Also, the catalytic activity of the NBGHSs is even better than those of the similar B- and N-doped graphene with non-spherical morphology.[30,32,62−64] This implies that the fabrication into the microspherical hollow structure could increase the electrochemical performance of the NBG as the catalyst for the ORR, which is in good agreement with our previously published work.[16] The specific microspherical hollow structure can not only promote the exposure of more active surface area accessible to the electrochemical reaction, but also decrease its overpotential for the ORR by reducing the contribution from the mass transport limitation.[16] Indeed, up to date, although much work has demonstrated that NBG can be used as electrocatalysts for the ORR, those with higher electrocatalytic activity than the JM Pt/C 40 wt % has less been reported. The higher electrocatalytic activity of the NBGHSs than that of the JM Pt/C 40 wt %, as demonstrated in Figure 4b, may further

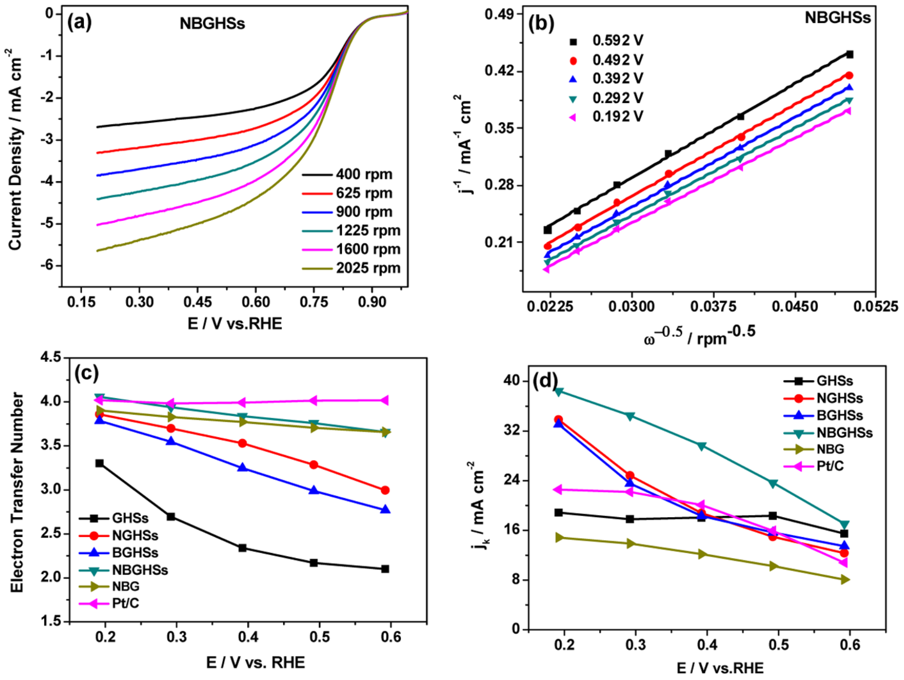

Figure 5. (a) Polarization curves at different potentials and (b) K-L plots of NBGHSs. (c) Dependence of the electron transfer number and (d) kinetic current density on the potential for the GHSs, the NGHSs, the BGHSs, the NBGHSs, the NBG, and the Pt/C 40 wt % in the O_2-saturated 0.1 M KOH.

suggest that fabrication of NBG into a microspherical hollow structure is a promising route to make its electrocatalytic activity higher than that of the JM Pt/C 40 wt %. On the basis of the results shown above, we would conclude that the high electrocatalytic activity of the NBGHSs arises from their specific microspherical hollow morphology and N, B codoped structure, both of which would greatly increase their performance as the electrocatalyst for the ORR.

To gain insight into the kinetics of electron transfer involved in the ORR of the NBGHSs, their LSVs in the O_2-saturated 0.1 M KOH solution under various electrode rotating rates were investigated. For comparison, the LSVs of the GHSs, the NGHSs, the BGHSs, the conventional NBG and the JM Pt/C 40 wt % in the O_2-saturated 0.1 M KOH solution under various electrode rotating rates were also measured. Figures 5a and S4 show enhancements of the measured current density with increase of the rotation rate for all the catalysts. The Koutechy–Levich (K-L) plots for all the catalysts at various electrode potentials in Figures 5b and S4 show linear relationships between J^{-1} and $\omega^{-0.5}$, indicating that the ORR catalyzed by these catalysts is of first order with respect to the concentration of the dissolved O_2 (see the Supporting Information for details). The transferred electron number (n) involved in the ORR on each catalyst can be then obtained using the slopes from the linear fitting of the K–L plots (see the Supporting Information for details).

The electrocatalytic ORR in an alkaline solution occurs either via a four-electron reduction pathway in which O_2 is directly reduced to H_2O or the two-electron reduction pathway where hydrogen peroxide (H_2O_2) is formed as an intermediate.[5,65] Generally, the four-electron reduction pathway is desired, because it provides a faster oxygen reduction rate. Figure 5c shows that for the ORR on the GHSs, the electron transfer number varies from 2.9 to 3.3 over the potential range covered in the present study, indicating that the two-electron transfer pathway plays a significant role in the ORR on the GHSs. The doping of N and B into the graphitic structure of the GHSs could both increases their electron transfer number for the ORR. As shown in Figure 5c, both of the NGHSs and BGHSs exhibit higher electron transfer numbers than the GHSs. This is consistent with the results reported previously that the heteroatom doping would facilitated the electrocatlytic reduction of oxygen by the graphene-based materials via a four-electron transfer pathway.[29,30,41,44] The most interesting is that the electron transfer number of the ORR on the NBGHSs is higher than those of both the NGHSs and BGHSs, as shown in Figure 5c. This indicates that there exists a synergistic effect between the N and B doping,[28,30,37,66] which leads to the higher electrocatalytic activity of the NBGHSs than those of both the NGHSs and BGHSs. The observation that the NBGHSs exhibit higher electron transfer number than the NBG suggests that the specific microspherical hollow structure is an addition reason, which leads to the higher electrochemical performance of the NBGHSs. These results are in good agreement with the conclusion drawn above that the higher electrocatalytic activity of the NBGHSs is the combining results of their specific microspherical hollow morphology and N, B codoped structure. In addition, Figure 5d also shows that the kinetic current density of the NBGHSs for the ORR is higher than those of the GHSs, NGHSs, BGHSs, and the NBG, indicating that the N, B codoped structure and the microspherical hollow morphology could also make the NBGHSs more kinetically facile toward ORR. Indeed, as shown in Figure 5d, the kinetic current density of the NBGHSs for the ORR is even higher than that of the JM Pt/C 40 wt %. This could be attributed to the reason that the NBGHSs can exhibit higher limiting current density and more positive half-wave potential than the JM Pt/C 40 wt %, although the electron transfer number for the ORR on the JM Pt/C 40 wt % is also close to 4 over the potential range covered in this study, as indicated in Figure 4b. The higher kinetic current density suggests that the NBGHSs are more kinetically facile than the Pt/C 40 wt % toward ORR. This is consistent with their relatively lower ORR Tafel slope (66 mV/decade) in comparison to that of the Pt/C 40 wt % (78 mV/decade), as shown in Figure 6 (the details on how the Tafel plots were obtained are given in the Supporting Information).

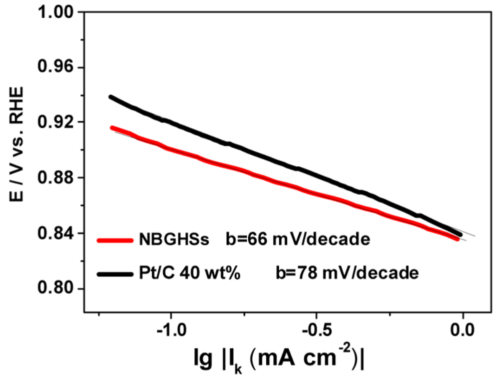

Figure 6. Tafel plots of the NBGHSs and the JM Pt/C derived by the mass-transport correction of corresponding RDE data (see the Supporting Information for details).

The results shown above suggest that the NBGHSs could be used as an efficient electrocatalyst for the ORR. To further demonstrate this, the stability and tolerance toward methanol and CO of the NBGHSs for ORR was measured. Figure 7 shows that the NBGHSs can remain highly active toward ORR with a loss of only 12% of their original activity over 10 h of the catalytic reaction and the introduction of methanol and CO shows no influence on their activity for the ORR. The stability and tolerance toward methanol and CO of the NBGHSs for ORR are much higher than the JM Pt/C 40 wt %. As shown in Figure 7a, a loss of more than 24% of the original ORR activity of the JM Pt/C 40 wt % could be observed after 10 h of the catalytic reaction, due to the dissociation of the Pt nanoparticles from the carbon substrate or the aggregation of the Pt nanoparticles during the electrochemical processes,[67−69] and the introduction of methanol and CO strongly decreases its activity for the ORR as shown in Figure 7b,c, due to the blockage of active sites on the Pt nanoparticles by the adsorption of CO or the methanol oxidation products.[70−72] The high stability and tolerance toward methanol and CO of the NBGHSs for ORR could be attributed to its specific molecular structure, which is highly stable and immune to the poisoning of methanol and CO, and the porous morphology of its randomly stacked solid, which can buffer the local structure change during the electrochemical ORR process. These results make us believe that the NBGHSs are the promising catalysts for the ORR with great potential to replace the commonly used noble-metal/C-based catalysts.

■ CONCLUSIONS

In summary, a simple template sacrificing method has been developed for the synthesis of the NBGHSs. These NBGHSs have been demonstrated to be highly active toward ORR and can exhibit even higher electrochemical performance than the commercial JM Pt/C 40 wt %. The high electrocatalytic activity of the NBGHSs could be attributed to the synergetic effect of the N, B codoped graphitic structure, which produces more active sites for the ORR, allowing the easier adsorption of oxygen and the subsequent reduction, and the specific microspherical hollow morphology, which promotes the exposure of more surface area accessible to electrolytes and decreases the overpotential for the ORR by reducing the contribution from the mass transport limitation. Along with

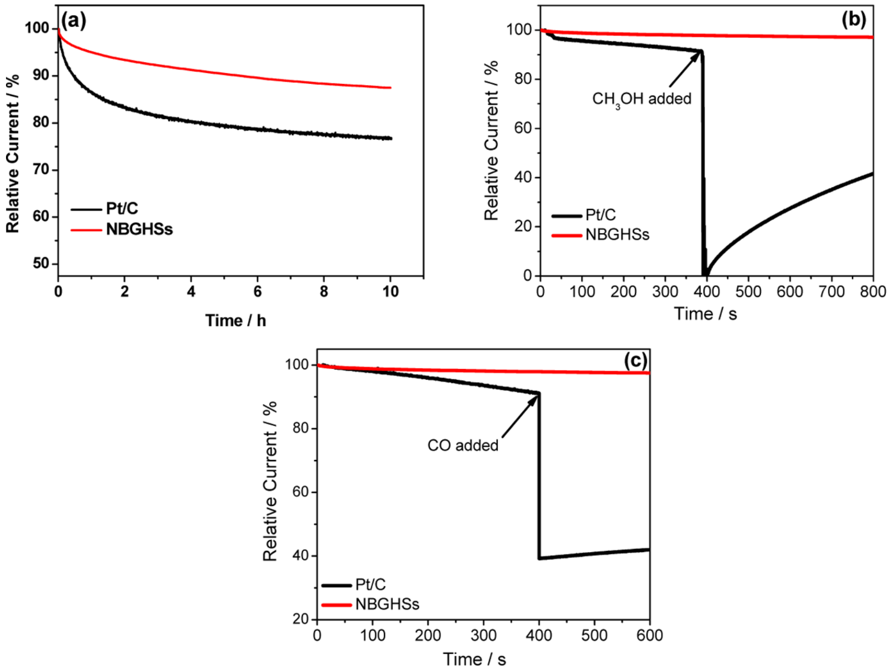

Figure 7. (a) Stability evaluation of the NBGHSs and the Pt/C 40 wt % electrodes for 10 h at 0.642 V vs RHE and a rotation rate of 1600 rpm. (b) Chronoamperometric responses in the O_2-saturated electrolyte for NBGHSs and the Pt/C 40 wt % catalysts by introducing 150 μL of methanol into the electrolyte at 400 s. (c) Chronoamperometric responses in the O_2-saturated electrolyte for NBGHSs and the Pt/C 40 wt % catalysts by introducing additional CO with the same flow of O_2 into the electrolyte at 400 s.

their low cost and good stability, the NBGHSs could be employed as an efficient electrocatalysts for the ORR with great promise to replace the commonly used metal/C catalysts. The work presented here therefore shows an additional promising strategy for the development of the advanced practical electrocatalysts for fuel cells.

■ ASSOCIATED CONTENT

Ⓢ Supporting Information

The Supporting Information is available free of charge on the ACS Publications website at DOI: 10.1021/acsami.5b05585.

> More detailed information regarding certain chemicals and reagents; calibration of SCE and conversion to RHE; rotating disk electrode (RDE) measurement; diffusion corrected Tafel plot; relative atomic percentages in the GHSs, the BGHSs, the NGHSs, and the NBGHSs analyzed based on the XPS spectra; SEM and TEM images of the GHSs, NGHSs, and BGHSs; CVs of GHSs, NGHSs, BGHSs, and NBG electrodes in nitrogen or oxygen saturated 0.1 M KOH solutions; polarization curves at different potentials and K-L plots of GHSs, NGHSs, BGHSs, and NBG (PDF).

■ AUTHOR INFORMATION

Corresponding Author

*Z.-J. Jiang. E-mail: zhongjiejiang1978@hotmail.com; eszjiang@scut.edu.cn.

Author Contributions

The paper was written through contributions of all authors. All authors have given approval to the final version of the paper.

Notes

The authors declare no competing financial interest.

■ ACKNOWLEDGMENTS

This work was financially supported by the “Outstanding Talent and Team Plans Program” of South China University of Technology, Fundamental Research Funds for the Central Universities of SCUT (No. 2014ZM0066), the Chinese National Natural Science Foundation (No. 11474101, 21306091 and 21376113), the Zhejiang Provincial Natural Science Foundation (No. LY14B030001), the Zhejiang Provincial Public Welfare Technology Application Research Project (2015C31151), the Ningbo Natural Science Foundation (No. 2014A610035), and Ningbo Science and Technology Innovation Team (2011B2002).

■ REFERENCES

(1) Jaouen, F.; Proietti, E.; Lefevre, M.; Chenitz, R.; Dodelet, J.-P.; Wu, G.; Chung, H. T.; Johnston, C. M.; Zelenay, P. Recent Advances in Non-Precious Metal Catalysis for Oxygen-Reduction Reaction in Polymer Electrolyte Fuel Cells. *Energy Environ. Sci.* **2011**, *4*, 114−130.

(2) Bezerra, C. W. B.; Zhang, L.; Lee, K.; Liu, H.; Marques, A. L. B.; Marques, E. P.; Wang, H.; Zhang, J. A Review of Fe−N/C And Co−N/C Catalysts for the Oxygen Reduction Reaction. *Electrochim. Acta* **2008**, *53*, 4937−4951.

(3) Wang, H.; Maiyalagan, T.; Wang, X. Review on Recent Progress in Nitrogen-Doped Graphene: Synthesis, Characterization, and Its Potential Applications. *ACS Catal.* **2012**, *2*, 781−794.

(4) Wang, Z.-L.; Xu, D.; Xu, J.-J.; Zhang, X.-B. Oxygen Electrocatalysts in Metal−Air Batteries: From Aqueous to Nonaqueous Electrolytes. *Chem. Soc. Rev.* **2014**, *43*, 7746−7786.

(5) Cheng, F.; Chen, J. Metal−Air Batteries: From Oxygen Reduction Electrochemistry to Cathode Catalysts. *Chem. Soc. Rev.* **2012**, *41*, 2172−2192.

(6) Aravind, S. S.; Ramaprabhu, S. Pt Nanoparticle-Dispersed Graphene-Wrapped MWNT Composites as Oxygen Reduction Reaction Electrocatalyst in Proton Exchange Membrane Fuel Cell. *ACS Appl. Mater. Interfaces* **2012**, *4* (8), 3805−3810.

(7) Wakabayashi, N.; Takeichi, M.; Uchida, H.; Watanabe, M. Temperature Dependence of Oxygen Reduction Activity at Pt-Fe, Pt-Co, and Pt-Ni Alloy Electrodes. *J. Phys. Chem. B* **2005**, *109*, 5836−5841.

(8) Liang, Y.; Li, Y.; Wang, H.; Zhou, J.; Wang, J.; Regier, T.; Dai, H. Co_3O_4 Nanocrystals on Graphene as a Synergistic Catalyst for Oxygen Reduction Reaction. *Nat. Mater.* **2011**, *10* (10), 780−786.

(9) Kim, J.; Lee, S. W.; Carlton, C.; Shao-Horn, Y. Pt-Covered Multiwall Carbon Nanotubes for Oxygen Reduction in Fuel Cell Applications. *J. Phys. Chem. Lett.* **2011**, *2* (11), 1332−1336.

(10) Winter, M.; Brodd, R. J. What Are Batteries, Fuel Cells, and Supercapacitors? *Chem. Rev.* **2004**, *104*, 4245−4269.

(11) Yu, X.; Ye, S. Recent Advances in Activity and Durability Enhancement of Pt/C Catalytic Cathode in PEMFC: Part II: Degradation Mechanism and Durability Enhancement of Carbon Supported Platinum Catalyst. *J. Power Sources* **2007**, *172*, 145−154.

(12) Singh, S. K.; Dhavale, V. M.; Kurungot, S. Low Surface Energy Plane Exposed Co3O4 Nanocubes Supported on Nitrogen-Doped Graphene as an Electrocatalyst for Efficient Water Oxidation. *ACS Appl. Mater. Interfaces* **2015**, *7*, 442−451.

(13) Qu, L.; Liu, Y.; Baek, J.-B.; Dai, L. Nitrogen-Doped Graphene as Efficient Metal-Free Electrocatalyst for Oxygen Reduction in Fuel Cells. *ACS Nano* **2010**, *4* (3), 1321−1326.

(14) Yang, W.; Fellinger, T.-P.; Antonietti, M. Efficient Metal-Free Oxygen Reduction in Alkaline Medium on High-Surface-Area Mesoporous Nitrogen-Doped Carbons Made from Ionic Liquids and Nucleobases. *J. Am. Chem. Soc.* **2011**, *133* (2), 206−209.

(15) Jiang, Z.; Jiang, Z.-j.; Tian, X.; Chen, W. Amine-Functionalized Holey Graphene as A Highly Active Metal-Free Catalyst for The Oxygen Reduction Reaction. *J. Mater. Chem. A* **2014**, *2*, 441−450.

(16) Jiang, Z.-J.; Jiang, Z. Reduction of the Oxygen Reduction Reaction Overpotential of Nitrogen-Doped Graphene by Designing It to A Microspherical Hollow Shape. *J. Mater. Chem. A* **2014**, *2*, 14071−14081.

(17) Zhang, J.; Zhao, Z.; Xia, Z.; Dai, L. A Metal-Free Bifunctional Electrocatalyst for Oxygen Reduction And Oxygen Evolution Reactions. *Nat. Nanotechnol.* **2015**, *10* (5), 444−452.

(18) Mao, S.; Wen, Z.; Huang, T.; Hou, Y.; Chen, J. High-Performance Bi-Functional Electrocatalysts of 3D Crumpled Graphene-Cobalt Oxide Nanohybrids for Oxygen Reduction And Evolution Reactions. *Energy Environ. Sci.* **2014**, *7* (2), 609−616.

(19) Choi, C. H.; Park, S. H.; Woo, S. I. Phosphorus−Nitrogen Dual Doped Carbon as An Effective Catalyst for Oxygen Reduction Reaction in Acidic Media: Effects of the Amount of P-Doping on the Physical And Electrochemical Properties of Carbon. *J. Mater. Chem.* **2012**, *22* (24), 12107−12115.

(20) Ma, G.; Jia, R.; Zhao, J.; Wang, Z.; Song, C.; Jia, S.; Zhu, Z. Nitrogen-Doped Hollow Carbon Nanoparticles with Excellent Oxygen Reduction Performances and Their Electrocatalytic Kinetics. *J. Phys. Chem. C* **2011**, *115* (50), 25148−25154.

(21) Chen, S.; Bi, J.; Zhao, Y.; Yang, L.; Zhang, C.; Ma, Y.; Wu, Q.; Wang, X.; Hu, Z. Nitrogen-Doped Carbon Nanocages as Efficient Metal-Free Electrocatalysts for Oxygen Reduction Reaction. *Adv. Mater.* **2012**, *24* (41), 5593−5597.

(22) Parvez, K.; Yang, S.; Hernandez, Y.; Winter, A.; Turchanin, A.; Feng, X.; Müllen, K. Nitrogen-Doped Graphene and Its Iron-Based Composite As Efficient Electrocatalysts for Oxygen Reduction Reaction. *ACS Nano* **2012**, *6*, 9541−9550.

(23) Hao, L.; Zhang, S.; Liu, R.; Ning, J.; Zhang, G.; Zhi, L. Bottom-Up Construction of Triazine-Based Frameworks as Metal-Free Electrocatalysts for Oxygen Reduction Reaction. *Adv. Mater.* **2015**, *27* (20), 3190−3195.

(24) Gong, K.; Du, F.; Xia, Z.; Durstock, M.; Dai, L. Nitrogen-Doped Carbon Nanotube Arrays with High Electrocatalytic Activity for Oxygen Reduction. *Science* **2009**, *323*, 760−764.

(25) Zhang, L.; Xia, Z. Mechanisms of Oxygen Reduction Reaction on Nitrogen-Doped Graphene for Fuel Cells. *J. Phys. Chem. C* **2011**, *115* (22), 11170−11176.

(26) Nam, G.; Park, J.; Kim, S. T.; Shin, D.-b.; Park, N.; Kim, Y.; Lee, J.-S.; Cho, J. Metal-Free Ketjenblack Incorporated Nitrogen-Doped Carbon Sheets Derived from Gelatin as Oxygen Reduction Catalysts. *Nano Lett.* **2014**, *14* (4), 1870−1876.

(27) Yang, L.; Jiang, S.; Zhao, Y.; Zhu, L.; Chen, S.; Wang, X.; Wu, Q.; Ma, J.; Ma, Y.; Hu, Z. Boron-Doped Carbon Nanotubes As Metal-Free Electrocatalysts for the Oxygen Reduction Reaction. *Angew. Chem., Int. Ed.* **2011**, *50* (31), 7132−7135.

(28) Wang, S.; Zhang, L.; Xia, Z.; Roy, A.; Chang, D. W.; Baek, J. B.; Dai, L. BCN Graphene as Efficient Metal-Free Electrocatalyst for the Oxygen Reduction Reaction. *Angew. Chem., Int. Ed.* **2012**, *51* (17), 4209−4212.

(29) Sheng, Z.-H.; Gao, H.-L.; Bao, W.-J.; Wang, F.-B.; Xia, X.-H. Synthesis of Boron Doped Graphene for Oxygen Reduction Reaction in Fuel Cells. *J. Mater. Chem.* **2012**, *22* (2), 390−395.

(30) Favaro, M.; Ferrighi, L.; Fazio, G.; Colazzo, L.; Di Valentin, C.; Durante, C.; Sedona, F.; Gennaro, A.; Agnoli, S.; Granozzi, G. Single and Multiple Doping in Graphene Quantum Dots: Unraveling the Origin of Selectivity in the Oxygen Reduction Reaction. *ACS Catal.* **2015**, *5* (1), 129−144.

(31) Kattel, S.; Atanassov, P.; Kiefer, B. Density Functional Theory Study of the Oxygen Reduction Reaction Mechanism in A BN Co-Doped Graphene Electrocatalyst. *J. Mater. Chem. A* **2014**, *2*, 10273−10279.

(32) Zheng, Y.; Jiao, Y.; Ge, L.; Jaroniec, M.; Qiao, S. Z. Two-Step Boron and Nitrogen Doping in Graphene for Enhanced Synergistic Catalysis. *Angew. Chem., Int. Ed.* **2013**, *52* (11), 3110−3116.

(33) Liang, J.; Jiao, Y.; Jaroniec, M.; Qiao, S. Z. Sulfur and Nitrogen Dual-Doped Mesoporous Graphene Electrocatalyst for Oxygen Reduction with Synergistically Enhanced Performance. *Angew. Chem., Int. Ed.* **2012**, *51* (46), 11496−11500.

(34) Yang, S.; Zhi, L.; Tang, K.; Feng, X.; Maier, J.; Müllen, K. Efficient Synthesis of Heteroatom (N or S)-Doped Graphene Based on Ultrathin Graphene Oxide-Porous Silica Sheets for Oxygen Reduction Reactions. *Adv. Funct. Mater.* **2012**, *22* (17), 3634−3640.

(35) Rao, C. N. R.; Gopalakrishnan, K.; Govindaraj, A. Synthesis, Properties and Applications of Graphene Doped with Boron, Nitrogen and Other Elements. *Nano Today* **2014**, *9* (3), 324−343.

(36) Wang, X.; Wang, J.; Wang, D.; Dou, S.; Ma, Z.; Wu, J.; Tao, L.; Shen, A.; Ouyang, C.; Liu, Q.; Wang, S. One-Pot Synthesis of Nitrogen And Sulfur Co-Doped Graphene as Efficient Metal-Free Electrocatalysts for the Oxygen Reduction Reaction. *Chem. Commun.* **2014**, *50*, 4839−4842.

(37) Zhang, Y.; Zhuang, X.; Su, Y.; Zhang, F.; Feng, X. Polyaniline Nanosheet Derived B/N Co-Doped Carbon Nanosheets as Efficient Metal-Free Catalysts for Oxygen Reduction Reaction. *J. Mater. Chem. A* **2014**, *2*, 7742−7746.

(38) Choi, C. H.; Chung, M. W.; Kwon, H. C.; Park, S. H.; Woo, S. I. B, N- And P, N-Doped Graphene as Highly Active Catalysts for Oxygen Reduction Reactions in Acidic Media. *J. Mater. Chem. A* **2013**, *1*, 3694−3699.

(39) Ma, Y.; Sun, L.; Huang, W.; Zhang, L.; Zhao, J.; Fan, Q.; Huang, W. Three-Dimensional Nitrogen-Doped Carbon Nanotubes/Graphene Structure Used as a Metal-Free Electrocatalyst for the Oxygen Reduction Reaction. *J. Phys. Chem. C* **2011**, *115* (50), 24592−24597.

(40) Bo, X.; Han, C.; Zhang, Y.; Guo, L. Confined Nanospace Synthesis of Less Aggregated and Porous Nitrogen-Doped Graphene As Metal-Free Electrocatalysts for Oxygen Reduction Reaction in Alkaline Solution. *ACS Appl. Mater. Interfaces* **2014**, *6*, 3023−3030.

(41) Zhou, X.; Bai, Z.; Wu, M.; Qiao, J.; Chen, Z. 3-Dimensional Porous N-Doped Graphene Foam as A Non-Precious Catalyst for the Oxygen Reduction Reaction. *J. Mater. Chem. A* **2015**, *3*, 3343−3350.

(42) Jiang, Z.-J.; Jiang, Z.; Chen, W. The Role of Holes in Improving the Performance of Nitrogen-Doped Holey Graphene as an Active Electrode Material for Supercapacitor And Oxygen Reduction Reaction. *J. Power Sources* **2014**, *251*, 55−65.

(43) Wang, J.; Wang, H.-S.; Wang, K.; Wang, F.-B.; Xia, X.-H. Ice Crystals Growth Driving Assembly of Porous Nitrogen-Doped Graphene for Catalyzing Oxygen Reduction Probed By In Situ Fluorescence Electrochemistry. *Sci. Rep.* **2014**, *4*, 6723.

(44) Chen, X.; Chen, X.; Xu, X.; Yang, Z.; Liu, Z.; Zhang, L.; Xu, X.; Chen, Y.; Huang, S. Sulfur-Doped Porous Reduced Graphene Oxide Hollow Nanosphere Frameworks as Metal-Free Electrocatalysts for Oxygen Reduction Reaction And as Supercapacitor Electrode Materials. *Nanoscale* **2014**, *6*, 13740−13747.

(45) Lei, Z.; Christov, N.; Zhao, X. S. Intercalation of Mesoporous Carbon Spheres Between Reduced Graphene Oxide Sheets for Preparing High-Rate Supercapacitor Electrodes. *Energy Environ. Sci.* **2011**, *4* (5), 1866.

(46) Grun, M.; Unger, K. K.; Matsumoto, A.; Tsutsumi, K. Novel Pathways for the Preparation of Mesoporous MCM-41 Materials: Control Of Porosity And Morphology. *Microporous Mesoporous Mater.* **1999**, *27*, 207−216.

(47) Hummers, W. S.; Offeman, R. E. Preparation of Graphitic Oxide. *J. Am. Chem. Soc.* **1958**, *80* (6), 1339−1339.

(48) Jiang, Z.; Zhao, X.; Fu, Y.; Manthiram, A. Composite Membranes Based on Sulfonated Poly(ether ether ketone) and SDBS-Adsorbed Graphene Oxide for Direct Methanol Fuel Cells. *J. Mater. Chem.* **2012**, *22* (47), 24862−24869.

(49) Li, Y.; Zhou, W.; Wang, H.; Xie, L.; Liang, Y.; Wei, F.; Idrobo, J.-C.; Pennycook, S. J.; Dai, H. An Oxygen Reduction Electrocatalyst Based on Carbon Nanotube-Graphene Complexes. *Nat. Nanotechnol.* **2012**, *7* (6), 394−400.

(50) Yang, J.; Lind, J. U.; Trogler, W. C. Synthesis of Hollow Silica and Titania Nanospheres. *Chem. Mater.* **2008**, *20*, 2875−2877.

(51) Agrawal, M.; Gupta, S.; Pich, A.; Zafeiropoulos, N. E.; Stamm, M. A Facile Approach to Fabrication of ZnO−TiO_2 Hollow Spheres. *Chem. Mater.* **2009**, *21*, 5343−5348.

(52) Jiang, Z.-J.; Jiang, Z. Fabrication of Nitrogen-Doped Holey Graphene Hollow Microspheres and Their Use as an Active Electrode Material for Lithium Ion Batteries. *ACS Appl. Mater. Interfaces* **2014**, *6*, 19082−19091.

(53) Kwon, K.-A.; Lim, H.-S.; Sun, Y.-K.; Suh, K.-D. a-Fe_2O_3 Submicron Spheres with Hollow and Macroporous Structures as High-Performance Anode Materials for Lithium Ion Batteries. *J. Phys. Chem. C* **2014**, *118*, 2897−2907.

(54) Jeong, H. M.; Lee, J. W.; Shin, W. H.; Choi, Y. J.; Shin, H. J.; Kang, J. K.; Choi, J. W. Nitrogen-Doped Graphene for High-Performance Ultracapacitors and the Importance of Nitrogen-Doped Sites at Basal Planes. *Nano Lett.* **2011**, *11* (6), 2472−2477.

(55) Wu, Z. S.; Winter, A.; Chen, L.; Sun, Y.; Turchanin, A.; Feng, X.; Mullen, K. Three-Dimensional Nitrogen And Boron Co-Doped Graphene for High-Performance All-Solid-State Supercapacitors. *Adv. Mater.* **2012**, *24* (37), 5130−5135.

(56) Wu, Z.-S.; Ren, W.; Xu, L.; Li, F.; Cheng, H.-M. Doped Graphene Sheets As Anode Materials with Superhigh Rate and Large Capacity for Lithium Ion Batteries. *ACS Nano* **2011**, *5* (7), 5463−5471.

(57) Cattelan, M.; Agnoli, S.; Favaro, M.; Garoli, D.; Romanato, F.; Meneghetti, M.; Barinov, A.; Dudin, P.; Granozzi, G. Microscopic View on a Chemical Vapor Deposition Route to Boron-Doped Graphene Nanostructures. *Chem. Mater.* **2013**, *25* (9), 1490−1495.

(58) Lee, S. W.; Yabuuchi, N.; Gallant, B. M.; Chen, S.; Kim, B.-S.; Hammond, P. T.; Shao-Horn, Y. High-Power Lithium Batteries from Functionalized Carbon-Nanotube Electrodes. *Nat. Nanotechnol.* **2010**, *5* (7), 531−537.

(59) Wen, Z.; Wang, X.; Mao, S.; Bo, Z.; Kim, H.; Cui, S.; Lu, G.; Feng, X.; Chen, J. Crumpled Nitrogen-Doped Graphene Nanosheets with Ultrahigh Pore Volume for High-Performance Supercapacitor. *Adv. Mater.* **2012**, *24*, 5610−5616.

(60) Wang, Z.-L.; Xu, D.; Wang, H.-G.; Wu, Z.; Zhang, X.-B. *In Situ* Fabrication of Porous Graphene Electrodes for High-Performance Energy Storage. *ACS Nano* **2013**, *7* (3), 2422−2430.

(61) Zhang, L.; Zhang, F.; Yang, X.; Long, G.; Wu, Y.; Zhang, T.; Leng, K.; Huang, Y.; Ma, Y.; Yu, A.; Chen, Y. Porous 3D Graphene-Based Bulk Materials with Exceptional High Surface Area And Excellent Conductivity for Supercapacitors. *Sci. Rep.* **2013**, *3*, 1408.

(62) Rao, C. N. R.; Gopalakrishnan, K.; Maitra, U. Comparative Study of Potential Applications of Graphene, MoS_2, and Other Two-Dimensional Materials in Energy Devices, Sensors, and Related Areas. *ACS Appl. Mater. Interfaces* **2015**, *7* (15), 7809−7832.

(63) Moses, K.; Kiran, V.; Sampath, S.; Rao, C. N. R. Few-Layer Borocarbonitride Nanosheets: Platinum-Free Catalyst for the Oxygen Reduction Reaction. *Chem. - Asian J.* **2014**, *9* (3), 838−843.

(64) Xue, Y.; Yu, D.; Dai, L.; Wang, R.; Li, D.; Roy, A.; Lu, F.; Chen, H.; Liu, Y.; Qu, J. Three-Dimensional B,N-Doped Graphene Foam as A Metal-Free Catalyst for Oxygen Reduction Reaction. *Phys. Chem. Chem. Phys.* **2013**, *15* (29), 12220−12226.

(65) Wiggins-Camacho, J. D.; Stevenson, K. J. Mechanistic Discussion of the Oxygen Reduction Reaction at Nitrogen-Doped Carbon Nanotubes. *J. Phys. Chem. C* **2011**, *115*, 20002−20010.

(66) Wang, S.; Iyyamperumal, E.; Roy, A.; Xue, Y.; Yu, D.; Dai, L. Vertically Aligned BCN Nanotubes as Efficient Metal-Free Electrocatalysts for the Oxygen Reduction Reaction: A Synergetic Effect by Co-Doping with Boron And Nitrogen. *Angew. Chem., Int. Ed.* **2011**, *50* (49), 11756−11760.

(67) Uchida, H.; Izumi, K.; Watanabe, M. Temperature Dependence of CO-Tolerant Hydrogen Oxidation Reaction Activity at Pt, Pt-Co, and Pt-Ru Electrodes. *J. Phys. Chem. B* **2006**, *110*, 21924−21930.

(68) Lee, H.-J.; Cho, M. K.; Jo, Y. Y.; Lee, K.-S.; Kim, H.-J.; Cho, E.; Kim, S.-K.; Henkensmeier, D.; Lim, T.-H.; Jang, J. H. Application of TGA Techniques to Analyze the Compositional and Structural Degradation of PEMFC MEAs. *Polym. Degrad. Stab.* **2012**, *97*, 1010−1016.

(69) Yu, Y.; Xin, H. L.; Hovden, R.; Wang, D.; Rus, E. D.; Mundy, J. A.; Muller, D. A.; Abruña, H. D. Three-Dimensional Tracking and Visualization of Hundreds of Pt-Co Fuel Cell Nanocatalysts During Electrochemical Aging. *Nano Lett.* **2012**, *12*, 4417−4423.

(70) Zhang, Y.; Huang, Q.; Zou, Z.; Yang, J.; Vogel, W.; Yang, H. Enhanced Durability of Au Cluster Decorated Pt Nanoparticles for the Oxygen Reduction Reaction. *J. Phys. Chem. C* **2010**, *114*, 6860−6868.

(71) Ge, Q.; Desai, S.; Neurock, M.; Kourtakis, K. CO Adsorption on Pt-Ru Surface Alloys and on the Surface of Pt-Ru Bulk Alloy. *J. Phys. Chem. B* **2001**, *105*, 9533−9536.

(72) Davies, J. C.; Tsotridis, G. Temperature-Dependent Kinetic Study of CO Desorption from Pt PEM Fuel Cell Anodes. *J. Phys. Chem. C* **2008**, *112*, 3392−3397.